

Distributed CVR in Unbalanced Distribution Systems With PV Penetration

Qianzhi Zhang¹, Student Member, IEEE, Kaveh Dehghanpour¹, Member, IEEE,
and Zhaoyu Wang¹, Member, IEEE

Abstract—In this paper, a distributed multi-objective optimization model is proposed to coordinate the fast-dispatch of photovoltaic (PV) inverters with the slow-dispatch of on-load tap changer and capacitor banks for implementing conservation voltage reduction in unbalanced three-phase distribution systems. In existing studies, PV inverters and voltage regulation devices are generally dispatched by fully centralized control frameworks. However, centralized optimization methods are subject to single point of failure and suffer large computational burden. To tackle these challenges, a distributed dispatch method is developed to coordinate PV inverters and conventional voltage regulation devices in distribution systems. The proposed method is based on a modified alternating direction method of multipliers algorithm to handle non-convex optimization problems without relaxing the original formulation, which could lead to sub-optimality. Numerical results from simulations on modified IEEE 13-bus, 34-bus, and 123-bus unbalanced three-phase systems have been used to verify the proposed method.

Index Terms—Conservation voltage reduction, distributed dispatch, multi-objective optimization, photovoltaic inverters, voltage regulation.

NOMENCLATURE

Sets and Indices

- Ω_N Set of buses
- Ω_i Set of buses connected to bus i
- Ω_T Set of dispatch period T
- Ω_ϕ Set of phases a, b, c .

Parameters

- α_i Unbalanced phase factor of bus i
- θ_{ib}, θ_{ic} Phase angle differences at bus i relative to phase angle θ_{ia}
- w_1, w_2 Weight factors in multi-objective optimization problem
- $P_{i,t,\phi}^{PV}$ Injected active power of PV of bus i , at time t , for phase ϕ

- $P_{i,t,\phi}^{pred}$ Predicted active power of PV of bus i , at time t , for phase ϕ
- $\varepsilon_{i,t,\phi}$ Prediction error of PV active power output of bus i , at time t , for phase ϕ
- $S_{i,t,\phi}^{PV}$ PV generation capacity of bus i , at time t , for phase ϕ
- q_i^{CB} CB unit reactive power output of bus i
- $z_{i,\phi}$ Impedance of the line connecting bus $i - 1$ to bus i for phase ϕ
- $r_{i,\phi}, x_{i,\phi}$ Resistance and reactance of the line connecting bus $i - 1$ to bus i for phase ϕ
- $q_{i,t,\phi}^*$ PV inverter reactive power generation or consumption capacity of bus i , at time t , for phase ϕ
- $V_{i,t}^{max}, V_{i,t}^{min}$ Maximum and minimum limits for nodal voltage of bus i
- Z_i^p, I_i^p, P_i^p Active ZIP load factors of bus i
- Z_i^q, I_i^q, P_i^q Reactive ZIP load factors of bus i
- CB^{max} Maximum limit for CB switching operation number during a certain dispatch period T
- TAP^{max} Maximum limit for OLTC tap changing number during a certain dispatch period T .

Variables

- $V_{i,t,\phi}$ Voltage magnitude of bus i , at time t , for phase ϕ
- $P_{i,t,\phi}^l, Q_{i,t,\phi}^l$ Active and reactive power flow of the line connecting bus $i - 1$ to bus i , at time t , for phase ϕ
- $Q_{i,t,\phi}^{PV}$ Injected reactive power of PV inverter of bus i , at time t , for phase ϕ
- $Q_{i,t}^{CB}$ Reactive power output of CB of bus i , at time t
- $P_{i,t,\phi}^{ZIP}, Q_{i,t,\phi}^{ZIP}$ Active and reactive ZIP load of bus i
- $I_{i,t}^{CB}, y_{i,t}^{CB}$ CB switching status variable and its auxiliary continuous variable of bus i , at time t
- I_t^{tap}, y_t^{tap} OLTC tap position variable and its auxiliary continuous variable of bus i , at time t
- $V_{i,t,\phi}^+, V_{i,t,\phi}^-$ Auxiliary voltage magnitude variables for $V_{i,t,\phi}$ and $V_{j,t,\phi}$
- $U_{i,t,\phi}^+, U_{i,t,\phi}^-$ Auxiliary variables for square of voltage magnitude variables $V_{i,t,\phi}$ and $V_{j,t,\phi}$
- $P_{i,t,\phi}^+, P_{i,t,\phi}^-$ Auxiliary active power flow variables for $P_{i,t,\phi}^l$ and $P_{j,t,\phi}^l$
- $Q_{i,t,\phi}^+, Q_{i,t,\phi}^-$ Auxiliary reactive power flow variables for $Q_{i,t,\phi}^l$ and $Q_{j,t,\phi}^l$

Manuscript received June 29, 2018; revised September 26, 2018; accepted November 6, 2018. This work was supported by the Power Systems Engineering Research Center under Project S-70. Paper no. TSG-00964-2018. (Corresponding author: Qianzhi Zhang.)

The authors are with the Department of Electrical and Computer Engineering, Iowa State University, Ames, IA 50011 USA (e-mail: qianzhi@iastate.edu; wzy@iastate.edu).

Color versions of one or more of the figures in this paper are available online at <http://ieeexplore.ieee.org>.

Digital Object Identifier 10.1109/TSG.2018.2880419

AQ1

80	$\lambda_{i,t,\phi}^{P+}, \lambda_{i,t,\phi}^{P-}$	Lagrange multipliers of auxiliary equality constraints for $P_{i,t,\phi}^{+}$ and $P_{i,t,\phi}^{-}$
81		
82	$\lambda_{i,t,\phi}^{Q+}, \lambda_{i,t,\phi}^{Q-}$	Lagrange multipliers of auxiliary equality constraints for $Q_{i,t,\phi}^{+}$ and $Q_{i,t,\phi}^{-}$
83		
84	$\lambda_{i,t,\phi}^{U+}, \lambda_{i,t,\phi}^{U-}$	Lagrange multipliers of auxiliary equality constraints for $U_{i,t,\phi}^{+}$ and $U_{i,t,\phi}^{-}$
85		
86	$\lambda_{i,t}^{y^{CB}}, \lambda_t^{y^{tap}}$	Lagrange multipliers of auxiliary equality constraints for $y_{i,t}^{CB}$ and y_t^{tap}
87		
88	$\lambda_i^{z1}, \lambda_i^{z2}$	Lagrange multipliers of auxiliary equality constraints $g_{z1,i}(\cdot)$ and $g_{z2,i}(\cdot)$.
89		

I. INTRODUCTION

CONSERVATION voltage reduction (CVR) is a viable technique used by utilities for peak shaving and long-term energy savings. CVR is achieved by controlled voltage level decrease of voltage-sensitive customers [1]. A conventional approach for implementing CVR is by adjusting tap positions of On-Load Tap Changer (OLTC) at the substation transformers, which ensures that the nodal voltages are reduced in a manner that neither violates the acceptable voltage ranges nor affects the performance of devices [2]. A more advanced way of implementation is to integrate CVR into Volt/VAr optimization (VVO) models as an objective function, which provide a framework for optimal control of voltage regulation and VAr control devices to achieve specific operational goals without violating any of the operational constraints.

VVO has been used for optimal control of conventional Volt/VAr regulation devices, such as capacitor banks (CBs) and OLTC [3], [4]. However, these conventional Volt/VAr regulation devices have slow reaction speed and limited number of switching operations, which cannot handle the fast changes in system states caused by increasing penetration of renewable energy resources (RES) in modern distribution systems. While the implementation of CVR requires a relatively flat voltage profile along the feeders in distribution systems, higher penetration levels of RES will cause fast and uncertain voltage fluctuations and deviations. On the other hand, PV smart inverters have much higher response speed and more flexible reactive power generation and absorption capabilities to handle fast voltage deviations caused by uncertain RES output and load fluctuations. Therefore, to improve the efficiency of voltage regulation and get a better performance for CVR implementation, modern VVO models are not only designed to include optimal control of conventional Volt/VAr regulation devices, but also control of PV smart inverters to facilitate voltage reduction [5]–[8].

In previous VVO studies, a multi-timescale voltage regulation framework has been frequently applied as shown in Fig. 1. This framework separates dispatching of conventional Volt/VAr regulation devices and PV inverters, as they take place on different timescales. Following this multi-timescale voltage regulation framework, hourly dispatch of OLTC, CBs and 15-min dispatch of PV inverters are coordinated in our research.

In general, three different optimization methods are applied in the multi-timescale VVO framework: 1) fully centralized

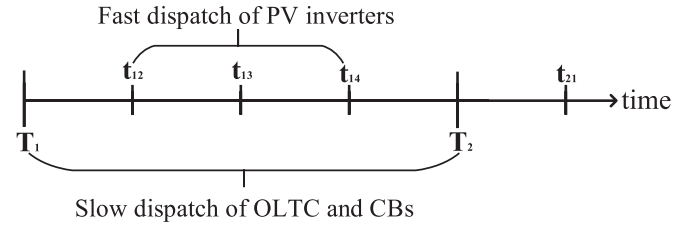


Fig. 1. Multi-timescale voltage regulation framework in VVO.

optimization methods, 2) hierarchical optimization methods, and 3) fully distributed optimization methods. In [5]–[7], the slow-dispatch of conventional voltage regulation devices and the fast-dispatch of PV inverters are both solved by centralized optimization methods. Centralized optimization requires the system-wide collection of data, and a costly communication infrastructure to enable information passing between a control center and regulation devices [9], [10]. Moreover, these methods are susceptible to single point of failure. Therefore, fully centralized optimization models are disadvantageous due to the increasing burden of computation in modern distribution systems with increasing size of decision models. A partial solution to this problem is to adopt a hierarchical optimization approach for VVO, as presented in [8], where the slow-dispatch of conventional voltage regulation devices is solved by a centralized optimization method, while a distributed optimization technique is used to solve the fast-dispatch of PV inverters. However, this VVO model divides the dispatching model into two optimization problems, which cannot guarantee the global optimality of the original optimization problem.

As discussed previously, fully centralized and hierarchical methods are both impractical in large interconnected and complex distribution systems. On the other hand, fully distributed optimization methods represent an economically viable and computationally simpler alternative to address the above-mentioned challenges [11]. Distributed methods are applied based on distributed optimization algorithms, which only rely on local data collection and local information exchange between neighboring control agents. Also, in contrast with centralized methods that have a single point of failure, distributed optimization techniques are resilient against agent communication failure and communication limits [12], [13]. Besides, in distributed approaches, the data privacy and ownership of customers are maintained, including local consumption measurement data and cost functions [14]. Thus, a large-scale optimization problem can be divided into a number of small-scale optimization problems, which are efficiently coordinated and solved by local agents to obtain a final solution for the original problem. In recent studies, distributed optimization methods have been largely applied to different power engineering applications, including distributed DC optimal power flow in power transmission systems [13], [15], as well as distributed optimal AC power flow in distribution networks [16], [17]. Distributed optimization methods are also applied to voltage regulation problems. For example, [18] introduces a VVO model which only controls the optimal set-points of OLTC devices, while [19] and [20] propose VVO models to optimally

182 dispatch PV inverters. Even though distributed optimization
 183 methods are applied in previous studies, the problem of
 184 PV inverter coordination with conventional voltage regulation
 185 devices using distributed optimization has remained largely
 186 unstudied, which leads to poor voltage regulation performance
 187 in the system.

188 To tackle this problem, in this paper a fully distributed
 189 method is proposed to optimally coordinate the slow-dispatch
 190 of conventional voltage regulation devices and the fast-
 191 dispatch of PV inverters in a unified optimization framework.
 192 The proposed distributed method in this research is developed
 193 based on alternating direction method of multipliers (ADMM).
 194 ADMM was originally applied to solve convex problems by
 195 minimizing the decomposed augmented Lagrangian function
 196 associated with each control area in an iterative way [21].
 197 However, control actions in VVO problems, such as the oper-
 198 ation statuses of CVs and tap position of OLTCs, can only
 199 be accurately modeled as discrete variables. Even though the
 200 existence of a theoretical convergence guarantees for ADMM
 201 in non-convex cases is still an open problem [22], some
 202 modifications to ADMM can be made to find local mini-
 203 mums for non-convex problem. A simple solution to address
 204 problem non-convexity is to perform optimization relaxation
 205 by replacing discrete variables with continuous variables in the
 206 distributed algorithm [23]. However, this approach may not be
 207 able to ensure a high quality solution. A more reasonable mod-
 208 ification method is proposed in [24] and used in this paper,
 209 where the discrete variables are not only replaced and relaxed
 210 by continuous variables, but also integrated into the ADMM
 211 objective function. This modified ADMM solver is able to
 212 avoid changing the structure of the original non-convex deci-
 213 sion model, which reduces the risk of solution sub-optimality.

214 When implementing CVR using VVO, the objective is
 215 usually set to minimize the bus voltage magnitudes with-
 216 out violating bus voltage limits to reduce power consump-
 217 tion. However, due to lower bus voltages, the system power
 218 losses will increase [25], which is in conflict with the gen-
 219 eral objective of VVO, i.e., minimization of system power
 220 losses. Therefore, VVO-based CVR implementation requires
 221 a trade-off between voltage reduction and real power loss
 222 reduction, which needs to be quantified. In this research,
 223 a multi-objective optimization formulation is developed to
 224 quantify this trade-off relationship. By changing the user-
 225 defined weight factors in the multi-objective function, the
 226 importance levels of bus voltage minimization for CVR and
 227 network power loss minimization will be controlled. The
 228 proposed method is tested on three test systems with dif-
 229 ferent number of nodes (IEEE 13-bus, 34-bus, and 123-bus
 230 systems). Numerical results show the superior performance
 231 of the proposed distributed optimization model compared to
 232 conventional centralized approaches in terms of computational
 233 speed and solution quality.

234 The main contributions of this research can be summarized
 235 as follows:

- 236 • An optimization model is developed to coordinate the
 237 fast-dispatch of PV inverters with the slow-dispatch of
 238 OLTC and CBs, in order to facilitate voltage reduction in
 239 unbalanced three-phase distribution systems.

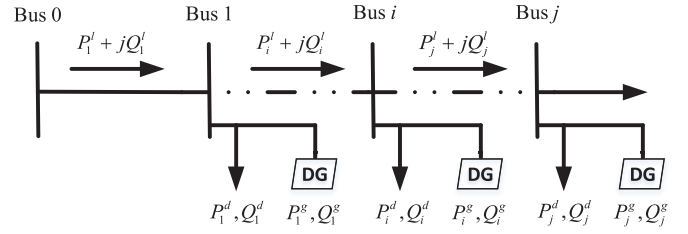


Fig. 2. Schematic diagram of a radial distribution system.

- 240 • In order to ensure the solution optimality and main- 240
 241 tain customer data privacy and ownership, a distributed 241
 242 solution methodology is proposed to dispatch all the 242
 243 above-mentioned devices in a unified optimization frame- 243
 244 work. The solution methodology is based on a modified 244
 245 ADMM technique to handle the non-convex optimization 245
 246 problem with discrete switching and tap changing 246
 247 variables. 247
- 248 • The trade-off between voltage reduction and real power 248
 249 loss reduction is quantified numerically using the devel- 249
 250 oped multi-objective VVO formulation. 250

251 The organization of this paper is as follows: Section III 251
 252 introduces the unbalanced three-phase distribution system 252
 253 model and formulates the optimal coordination of PV invert- 253
 254 ers with OLTC and CBs. Section IV discusses the modified 254
 255 ADMM to handle non-convex discrete variables, and shows 255
 256 the operation of the modified ADMM. Simulation results and 256
 257 conclusions are presented in Sections V and VI, respectively. 257

258 II. CENTRALIZED COORDINATION OF PVs WITH 258 259 CONVENTIONAL VOLTAGE REGULATION DEVICES 259

260 In this section, we develop a multi-objective optimization 260
 261 model to coordinate the fast-dispatch of PV inverters with 261
 262 the slow-dispatch of OLTC and CBs in unbalanced three-phase 262
 263 distribution systems. The DistFlow equations and ZIP load 263
 264 models are also introduced. The presented model in this sec- 264
 265 tion will be then used in Section IV to design a distributed 265
 266 solution strategy for VVO-based CVR. 266

267 A. Distribution System Model 267

268 To obtain the power flow solution in a radial distri- 268
 269 bution network, the DistFlow equations have been widely 269
 270 used [26], [27]. A typical radial distribution system is shown 270
 271 in Fig. 2, where the bus indexes are denoted as $i =$ 271
 272 $\{0, 1, 2, \dots, n\}$. 272

273 The DistFlow equations can be presented as 273
 274 equations (1)-(5). In (1)-(3) the nonlinear terms are much 274
 275 smaller than the linear terms and can be ignored. In practice, 275
 276 this linear form of DistFlow has been verified in many 276
 277 previous studies such as [20], [27]. 277

$$278 P_{i+1}^l = P_i^l - r_i \frac{(P_i^l)^2 + (Q_i^l)^2}{V_i^2} - p_{i+1} \quad (1)$$

$$279 Q_{i+1}^l = Q_i^l - x_i \frac{(Q_i^l)^2 + (P_i^l)^2}{V_i^2} - q_{i+1} \quad (2)$$

TABLE I
ZIP COEFFICIENTS FOR EACH CUSTOMER TYPE [28]

Bus Type	Zp	Ip	Pp	Zq	Iq	Pq
Commercial	0.43	-0.06	0.63	4.06	-6.65	4.49
Residential	0.85	-1.12	1.27	10.96	-18.73	8.77
Industrial	0	0	1	0	0	1

$$V_{i+1}^2 = V_i^2 - \frac{2(r_i P_i^l + x_i Q_i^l)}{V_s} + (r_i^2 + x_i^2) \frac{(P_i^l)^2 + (Q_i^l)^2}{V_i^2} \quad (3)$$

In (4) and (5), P_{i+1}^g is the active power generated by PVs at bus $i+1$. Q_{i+1}^g is the reactive power generated by VAR compensation devices at bus $i+1$. In the proposed model, PV inverters and CBs are considered as reactive power sources. P_{i+1}^d and Q_{i+1}^d are active power and reactive demand load at bus $i+1$, which will be modeled as ZIP active and reactive loads (refer to Section II-C).

$$p_{i+1} = P_{i+1}^d - P_{i+1}^g \quad (4)$$

$$q_{i+1} = Q_{i+1}^d - Q_{i+1}^g \quad (5)$$

B. Extension to Unbalanced Systems

To better model distribution systems, we will extend the power flow model to unbalanced three-phase systems using a simplified model [19], which can approximate phase imbalances. It is assumed that the voltage magnitudes of the three phases at bus i are similar, so that $|V_{i_a}| \approx |V_{i_b}| \approx |V_{i_c}|$. Then with the voltage phase angles $\theta_{i_a} = 0$, θ_{i_b} , and θ_{i_c} , the relative phase unbalance α_i is approximated as follows:

$$\alpha_i = [1, e^{j\theta_{i_b}}, e^{j\theta_{i_c}}]^T \quad (6)$$

Therefore, we can apply the relative phase unbalance α_i of bus i as follows: the equivalent unbalanced three-phase system line impedance $z_{i,\phi}$ can be calculated in (7) based on α_i and line impedance z_i . The real and imaginary parts of $z_{i,\phi}$ are the unbalanced three-phase system line resistance $r_{i,\phi}$ in (8) and unbalanced three-phase system line reactance $x_{i,\phi}$ in (9), respectively. Therefore, the DistFlow equations (1)-(3) can be extended to unbalanced three-phase by replacing $r_{i,\phi}$ and $x_{i,\phi}$ in (8)-(9). The load applied in this paper is also unbalanced.

$$z_{i,\phi} = \alpha_i \alpha_i^H \odot z_i \quad (7)$$

$$r_{i,\phi} = \text{real}(z_{i,\phi}) \quad (8)$$

$$x_{i,\phi} = \text{imag}(z_{i,\phi}) \quad (9)$$

C. ZIP Load Model

In our VVO formulations, the loads are represented using ZIP load models which include constant-impedance (Z), constant-current (I), and constant-power components (P). Z_i^p , I_i^p , P_i^p and Z_i^q , I_i^q , P_i^q are constant-impedance coefficients, constant-current coefficients and constant-power coefficients for active and reactive loads, respectively. In [28] and [29] typical ZIP coefficients for different types of customers, such as residential customers, commercial customers and industrial customers, have been provided. The ZIP coefficients in Table I (adopted from [28]) are used in this paper.

D. Centralized Coordination Model

In this section, a centralized optimization model is presented to coordinate the fast-dispatch of PV inverters and the slow-dispatch of conventional voltage regulation devices (OLTC and CBs) to facilitate voltage reduction in unbalanced distribution systems. This model will be decomposed into bus-level sub optimization problems in Section IV to design a distributed ADMM-based solver. The status of CBs and OLTC are scheduled at the beginning of every hour to manage the slow voltage variations, then the on-off status of CBs and tap of OLTCs are fixed for the rest of this hour within the optimization solver. In other words, no intra-hour decision instant is defined for CBs and OLTC. Within each hour, PV inverters are dispatched every 15 minutes to handle the faster voltage deviations. Hence, intra-hour decision instants are defined for PV inverters.

$$\min_{V_i, P_i, Q_i} \left(w_1 \sum_{i=1}^N (V_{i,\phi}^*) + w_2 \sum_{i=1}^N (\text{loss}_{i,\phi}) \right) \quad (10)$$

s.t.

$$V_{i,\phi}^* \geq \max_{t \in T} (V_{i,t,\phi}) \quad (11)$$

$$\text{loss}_{i,\phi} = \sum_{t=1}^T \left(r_{i,\phi} \frac{(P_{i,t,\phi}^l)^2 + (Q_{i,t,\phi}^l)^2}{V_s^2} \right) \quad (12)$$

$$P_{i,t,\phi}^l = P_{i-1,t,\phi}^l - P_{i,t,\phi}^{\text{ZIP}} + P_{i,t,\phi}^{\text{pred}} \quad (13)$$

$$P_{i,t,\phi}^{\text{PV}} = P_{i,t,\phi}^{\text{pred}} - \varepsilon_{i,t,\phi} \quad (14)$$

$$Q_{i,t,\phi}^l = Q_{i-1,t,\phi}^l - Q_{i,t,\phi}^{\text{ZIP}} + Q_{i,t,\phi}^{\text{PV}} + Q_{i,t,\phi}^{\text{CB}} \quad (15)$$

$$-q_{i,t,\phi}^* \leq Q_{i,t,\phi}^{\text{PV}} \leq q_{i,t,\phi}^* \quad (16)$$

$$q_{i,t,\phi}^* = \sqrt{(S_{i,t,\phi}^{\text{PV}})^2 - (P_{i,t,\phi}^{\text{pred}})^2} \quad (17)$$

$$Q_{i,t,\phi}^{\text{CB}} = I_{i,t,\phi}^{\text{CB}} q_i^{\text{CB}} \quad (18)$$

$$P_{i,t,\phi}^{\text{ZIP}} = P_{i,t,\phi}^{\text{D}} \left(Z_i^p V_{i,t,\phi}^2 + I_i^p V_{i,t,\phi} + P_i^p \right) \quad (19)$$

$$Q_{i,t,\phi}^{\text{ZIP}} = Q_{i,t,\phi}^{\text{D}} \left(Z_i^q V_{i,t,\phi}^2 + I_i^q V_{i,t,\phi} + P_i^q \right) \quad (20)$$

$$V_{i,t,\phi} = V_{i-1,t,\phi} - \frac{r_{i-1,\phi} P_{i-1,t,\phi}^l + x_{i-1,\phi} Q_{i-1,t,\phi}^l}{V_s} \quad (21)$$

$$V_{1,t} = V_s + I_t^{\text{tap}} V^{\text{tap}} \quad (22)$$

$$V_{i,t}^{\text{min}} \leq V_{i,t,\phi} \leq V_{i,t}^{\text{max}} \quad (23)$$

$$\sum_{t \in T} |I_{i,t}^{\text{CB}} - I_{i,t-1}^{\text{CB}}| \leq \text{CB}^{\text{max}} \quad (24)$$

$$\sum_{t \in T} |I_t^{\text{tap}} - I_{t-1}^{\text{tap}}| \leq \text{TAP}^{\text{max}} \quad (25)$$

$$I_{i,t}^{\text{CB}} \in \{0, 1\} \quad (26)$$

$$I_t^{\text{tap}} \in \{-10, -9, \dots, 0, \dots, 9, 10\} \quad (27)$$

$$\forall i \in \Omega_N, \forall t \in \Omega_T, \forall \phi \in \Omega_\phi \quad (28)$$

In the above formulations, $V_{i,t,\phi}$, $P_{i,t,\phi}^l$, $Q_{i,t,\phi}^l$, as well as other variables and parameters are modeled in three-phase, e.g., $V_{i,t,\phi} = [V_{i_a,t}, V_{i_b,t}, V_{i_c,t}]^T$. The same applies to network parameters, e.g., $r_{i,\phi}, x_{i,\phi} \in \Omega^{3 \times 3}$.

In order to investigate the trade-off between the voltage (or load) reduction and real power loss reduction, we have included two components in the objective function (10): one component is aimed at minimization of the largest bus voltage and the other is defined to minimize the active line losses during the dispatch period. It is assumed that the two components are weighted by factors w_1 and w_2 ($0 \leq w_1, w_2 \leq 1$, $w_1 + w_2 = 1$), respectively. The distribution system operators can adjust the weighting factors w_1 and w_2 according to specific operational requirements.

Constraint (11) aims to find the largest voltage magnitude at bus i at time t . Equation (12) determines the overall active power losses on the line connecting bus i and bus $i - 1$ at t . Equation (13) is the nodal active power balance formulation, which includes the active power in-flow and out-flow at bus i , active power output of PV inverter, as well as the ZIP active load of bus i . Here, the reactive power outputs of PV inverters ($Q_{i,t,\phi}^{PV}$) will be dispatched considering the predicted active solar PV generation ($P_{i,t,\phi}^{pred}$). The uncertainty of PV power is represented by Gaussian random variables for PV power prediction error. Accordingly, each agent predicts the available nodal PV power over the decision window. Due to the uncertainty of PV power in real-time, the predicted value is different from the actual PV power. The difference is modeled using a Gaussian error variable as shown in equation (14), where $P_{i,t,\phi}^{pred}$ and $P_{i,t,\phi}^{PV}$ denote the predicted and actual active power output of PV, $\varepsilon_{i,t,\phi} \sim N(0, \sigma)$ denotes the Gaussian prediction error. The standard deviation of the error variable, ε , is chosen based on [30]. Note that the optimization problem is solved using the predicted PV power. Hence, the prediction error, which reflects the impact of PV power uncertainty, leads to slight deviation (less than 1%) from the true optimal solution. This deviation depends mainly on the quality of the prediction captured by the prediction error standard deviation. Equation (15) is the nodal reactive power balance formulation, which determines the reactive power output of PV inverter at bus i and reactive power output of CB at bus i . Constraint (16) and equation (17) limit the reactive power capacity of PV inverters based on PV generation capacity and the active power output. Combining constraints (15), (16) and (17), we can obtain (26) and (27). Now we can obtain $Q_{i,t,\phi}^{PV}$ by using the optimal results and the nodal reactive power balance equations.

$$Q_{i,t,\phi}^I - Q_{i-1,t,\phi}^I + Q_{i,t,\phi}^{ZIP} - Q_{i,t}^{CB} - q_{i,t}^* \leq 0 \quad (26)$$

$$-Q_{i,t,\phi}^I + Q_{i-1,t,\phi}^I - Q_{i,t,\phi}^{ZIP} + Q_{i,t}^{CB} - q_{i,t}^* \leq 0 \quad (27)$$

Equation (18) obtains the CB reactive power injection at bus i . $I_{i,t}^{CB}$ represents the on/off status of the CB at bus i during the dispatch period T . For buses without CB, q_i^{CB} is set to zero. Equations (19) and (20) represent the ZIP active and reactive load by second-order polynomial formulations. Summation of ZIP coefficients for both active and reactive are set to 1. $P_{i,t,\phi}^D$ and $Q_{i,t,\phi}^D$ are active and reactive power demand factors during the dispatch period, respectively. Equation (21) determines the bus voltage using DistFlow equations.

Equation (22) determines the substation transformer secondary voltage according to primary voltage V_s and OLTC tap position I_t^{tap} . Constraint (23) guarantees that the bus voltage is

maintained within the allowable range, and the voltage limits are set to be [0.95, 1.05]. Constraints (24) and (25) denote the maximum allowable switching actions of CBs and OLTC during the dispatch period. For example, in the following case studies, the CB^{max} is set to be 3 and TAP^{max} is set to be 5. In order to reduce the non-linearity of the absolute values, constraints (24)-(25) are transformed into linear forms.

III. DISTRIBUTED OPTIMIZATION METHOD

In this section, the centralized coordination model of PVs with OLTC and CBs is decomposed into bus-level sub-problems. A modified ADMM is introduced to handle the non-convex problem with discrete variables of CBs and OLTC.

A. Modified ADMM

Discrete variables $I_{i,t}^{CB}$ and I_t^{tap} are used in the centralized VVO formulations (10)-(25). However, the conventional ADMM is originally developed to solve convex problems. A simple solution to address this problem is to relax the discrete variables to continuous ones. However, this approach cannot ensure a high-quality solution in general. Instead, in [24] a modified ADMM has been proposed, which includes the auxiliary equality constraints with discrete variables as of the optimization objective function, and finds the best match for discrete variables in the ADMM iterative update process. Numerical results have shown that this modified ADMM has better performance in handling discrete variables compared to simple relax-and-round methods [24].

Considering the optimization problem (28)-(30), first, discrete variable I is replaced with an auxiliary continuous variable y in constraint (29); then, an additional auxiliary equality is introduced as constraint (30).

$$\min_{x,I} f(x, I) \quad (28)$$

s.t.

$$I = y \quad (29)$$

$$z = g(x, y) \quad (30)$$

$$I \in \mathbb{Z}, x, y \in \mathbb{R}$$

After decomposition, the augmented Lagrangian for this problem is shown in (31), where $\rho > 0$ is the penalty coefficient.

$$\mathcal{L}_\rho = f(x_i, y_i) + \lambda_i^z (z_i - g(x_i, I_i)) + \frac{\rho}{2} \|z_i - g(x_i, I_i)\|_2^2 \quad (31)$$

Therefore, the modified ADMM iterative update rules (32)-(34) for optimization problem (28)-(30) can be presented as follows (with the iteration number denoted by k):

$$(x_i(k+1), y_i(k+1)) = \underset{x,y}{\operatorname{argmin}} \mathcal{L}_\rho(x_i, y_i, \lambda_i^z(k)) \quad (32)$$

$$I_i(k+1) = \underset{I}{\operatorname{argmin}} \|z_i(k+1) - g(x_i(k+1), I_i)\|_2^2 \quad (33)$$

$$\lambda_i^z(k+1) = \lambda_i^z(k) + \rho(z_i(k+1) - g(x_i(k+1), I_i(k+1))). \quad (34)$$

B. Distributed Solution Algorithm

The centralized optimization problem (10)-(25) can be decomposed to a set of bus-level small-size optimization problems. Bus-level control agents are in charge of managing the local controllable resources and local voltage at each bus. This takes place through sharing estimated local solutions with neighboring agents using the proposed modified ADMM solution strategy. Each bus agent solves a local optimization problem, which has its own *local variables* $P_{i,t,\phi}^l, Q_{i,t,\phi}^l, V_{i,t,\phi}$, as well as the *copy variables* $P_{j,t,\phi}^l, Q_{j,t,\phi}^l, V_{j,t,\phi}$ exchanged between neighboring buses j to bus i . The buses installed with CBs or OLTC have discrete variables $I_{i,t}^{CB}$ and I_t^{tap} .

Therefore, with auxiliary variables and equality constraints, the original optimization problem can be decomposed into bus-level optimization problems. The constraints (11)-(25) can be reformulated as (11)*-(25)* by replacing the variables by their corresponding auxiliary variables.

$$\min_{U_i, P_i, Q_i} f(X_i, I_i) \quad (35)$$

s.t.

$$P_{i,t,\phi}^l = P_{i,t,\phi}^+, P_{j,t,\phi}^l = P_{i,t,\phi}^- \quad (36)$$

$$Q_{i,t,\phi}^l = Q_{i,t,\phi}^+, Q_{j,t,\phi}^l = Q_{i,t,\phi}^- \quad (37)$$

$$V_{i,t,\phi}^2 = U_{i,t,\phi} = U_{i,t,\phi}^+, V_{j,t,\phi}^2 = U_{j,t,\phi} = U_{i,t,\phi}^- \quad (38)$$

$$I_{i,t}^{CB} = y_{i,t}^{CB}, I_t^{tap} = y_t^{tap} \quad (39)$$

$$z_{1,i} = g_1(X_i, y_{i,t}^{CB}) \quad (40)$$

$$z_{2,i} = g_2(X_i, y_t^{tap}) \quad (41)$$

$$(11)^* - (25)^*$$

$$\forall i \in \Omega_N, \forall j \in \Omega_i, \forall t \in \Omega_T, \forall \phi \in \Omega_\phi$$

For convenience, four variable sets are defined at each bus to exchange information with agents at neighboring buses. Let the variable set X_i include $P_{i,t,\phi}^+, P_{i,t,\phi}^-, Q_{i,t,\phi}^+, Q_{i,t,\phi}^-, U_{i,t,\phi}^+, U_{i,t,\phi}^-$, the variable set I_i include $I_{i,t}^{CB}, I_t^{tap}$, the variable set Y_i include $y_{i,t}^{CB}, y_t^{tap}$ and the variable set λ_i include $\lambda_{i,t,\phi}^{P+}, \lambda_{i,t,\phi}^{P-}, \lambda_{i,t,\phi}^{Q+}, \lambda_{i,t,\phi}^{Q-}, \lambda_{i,t,\phi}^{U+}, \lambda_{i,t,\phi}^{U-}, \lambda_{i,t}^{y^{CB}}, \lambda_{i,t}^{y^{tap}}, \lambda_i^{z1}, \lambda_i^{z2}$.

To apply the modified ADMM to the proposed centralized coordination model (35)-(41) and (11)* - (25)*, the distributed iterative process has been presented as (42)-(57) in four steps. Fig. 3 shows the process of local optimization solution exchanges between neighboring bus agents in the distributed algorithm. The convergence criteria is set by a maximum iteration limit.

Step 1: For each bus agent i at iteration k , local optimization problems, shown in (42), are solved independently and in parallel. Solutions to bus local variables X_i and Y_i are obtained.

$$(X_i(k+1), Y_i(k+1)) = \operatorname{argmin}_{X,Y} \mathcal{L}_\rho(X_i, Y_i, \lambda_i(k)). \quad (42)$$

Step 2: For each bus agent i at iteration k , local optimization solution exchanges take place between neighboring agents to update variables based on respective bus local variables and variables at buses connected to bus i , which are obtained from step 1.

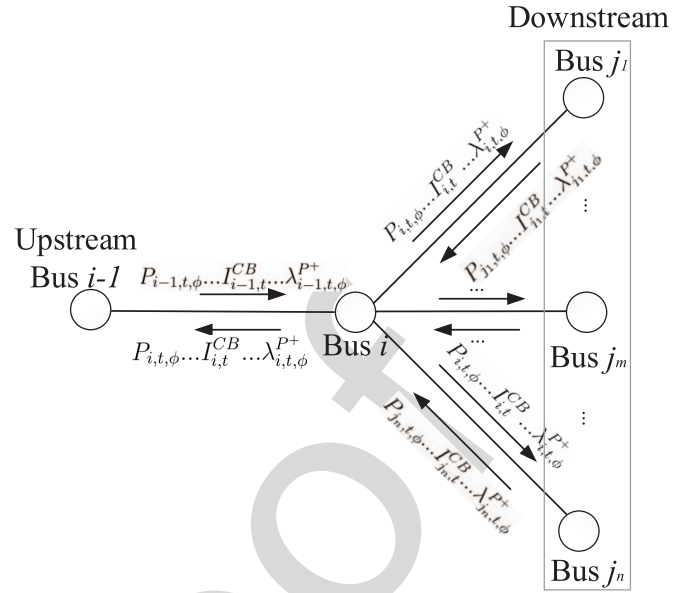


Fig. 3. Local optimization solution exchange between control agents at different buses.

Hence, variable set X_i is updated by averaging the respective local bus variables and using (43)-(45), where n_i denotes the number of buses connected to bus i plus 1:

$$P_{i,t,\phi}^l(k+1) = \frac{1}{2} \left(P_{i,t,\phi}^+(k+1) + P_{i,t,\phi}^-(k+1) \right) \quad (43)$$

$$Q_{i,t,\phi}^l(k+1) = \frac{1}{2} \left(Q_{i,t,\phi}^+(k+1) + Q_{i,t,\phi}^-(k+1) \right) \quad (44)$$

$$U_{i,t,\phi}(k+1) = \frac{1}{n_i} \left(U_{i,t,\phi}^+(k+1) + \dots + U_{i,t,\phi}^-(k+1) \right) \quad (45)$$

Variables $I_{i,t}^{CB}$ and I_t^{tap} are updated by solving local bus optimization problems using $X_i(k+1)$ and $Y_i(k+1)$ as shown in (46) and (47):

$$I_{i,t}^{CB}(k+1) = \operatorname{argmin}_{I_{i,t}} \left\| z_{1,i}(k+1) - g_1(X_i(k+1), I_{i,t}^{CB}) \right\|_2^2 \quad (46)$$

$$I_t^{tap}(k+1) = \operatorname{argmin}_{I_t} \left\| z_{1,i}(k+1) - g_2(X_i(k+1), I_t^{tap}) \right\|_2^2 \quad (47)$$

Step 3: For each bus i at iteration k , the Lagrange multipliers are updated based on the ADMM iterative rules and the variables obtained in previous steps. Hence, the Lagrange multipliers for variable set X_i are updated using (48)-(53):

$$\lambda_{i,t,\phi}^{P+}(k+1) = \lambda_{i,t,\phi}^{P+}(k) + \rho \left(P_{i,t,\phi}^+(k+1) - P_{i,t,\phi}^l(k+1) \right) \quad (48)$$

$$\lambda_{i,t,\phi}^{P-}(k+1) = \lambda_{i,t,\phi}^{P-}(k) + \rho \left(P_{i,t,\phi}^-(k+1) - P_{j,t,\phi}^l(k+1) \right) \quad (49)$$

$$\lambda_{i,t,\phi}^{Q+}(k+1) = \lambda_{i,t,\phi}^{Q+}(k) + \rho \left(Q_{i,t,\phi}^+(k+1) - Q_{i,t,\phi}^l(k+1) \right) \quad (50)$$

$$\lambda_{i,t,\phi}^{Q-}(k+1) = \lambda_{i,t,\phi}^{Q-}(k) + \rho \left(Q_{i,t,\phi}^-(k+1) - Q_{j,t,\phi}^l(k+1) \right) \quad (51)$$

$$\lambda_{i,t,\phi}^{U^+}(k+1) = \lambda_{i,t,\phi}^{U^+}(k) + \rho \left(U_{i,t,\phi}^+(k+1) - U_{i,t,\phi}(k+1) \right) \quad (52)$$

$$\lambda_{i,t,\phi}^{U^-}(k+1) = \lambda_{i,t,\phi}^{U^-}(k) + \rho \left(U_{i,t,\phi}^-(k+1) - U_{j,t,\phi}(k+1) \right) \quad (53)$$

Lagrange multipliers for auxiliary equality constraints corresponding to Y_i and I_i are updated using (54) and (55):

$$\lambda_{i,t}^{y^{CB}}(k+1) = \lambda_{i,t}^{y^{CB}}(k) + \rho \left(y_{i,t}^{CB}(k+1) - I_{i,t}^{CB}(k+1) \right) \quad (54)$$

$$\lambda_{i,t}^{y^{tap}}(k+1) = \lambda_{i,t}^{y^{tap}}(k) + \rho \left(y_{i,t}^{tap}(k+1) - I_{i,t}^{tap}(k+1) \right) \quad (55)$$

Lagrange multipliers for auxiliary equality constraints $g_1(\cdot)$ and $g_2(\cdot)$ are updated using (56) and (57):

$$\lambda_i^{z_1^1}(k+1) = \lambda_i^{z_1^1}(k) + \rho \left(z_{1,i}(k+1) - g_1 \left(X_i(k+1), I_{i,t}^{CB}(k+1) \right) \right) \quad (56)$$

$$\lambda_i^{z_1^2}(k+1) = \lambda_i^{z_1^2}(k) + \rho \left(z_{2,i}(k+1) - g_2 \left(X_i(k+1), I_{i,t}^{tap}(k+1) \right) \right). \quad (57)$$

Step 4: Increase k by 1 till it reaches the maximum iteration number.

IV. CASE STUDY

In this section, the convergence analysis and simulation results of our proposed method are presented. First, we present the convergence analysis to show the impact of different penalty parameter ρ on convergence speed. We then demonstrate the effectiveness of our proposed method through numerical evaluations on three IEEE standard benchmarks to study load/loss reduction through CVR implementation. Comparison between centralized optimization and proposed distributed optimization is also provided. All the case studies are simulated using a PC with Intel Core i7-4790 3.6 GHz CPU and 16 GB RAM hardware. The simulations are performed in MATLAB and GAMS to solve and update local variables in the iterative distributed optimization process. The main benefit of CVR for utilities is peak loading relief of distribution networks [31]–[33]. In this paper, the CVR is used for peak load reduction by modifying the voltages of the system buses through finding optimal switching and control actions for CBs and OLTCs, as well as reactive power injection/absorption set points for PV inverters. Given the voltage-sensitivity of active power (see the ZIP coefficients) these control actions, if chosen correctly, lead to a drop in consumption at critical times, such as the peak interval. In all the simulations, the CVR functionality was tested over 3 hours of peak load period with 15-minute time steps.

A. Case I: Convergence Analysis (IEEE 13-Bus System)

In order to perform convergence studies, the proposed method is implemented on IEEE 13-bus system and the results are recorded at each iteration. Fig. 4 shows the convergence results for different values of ρ . Within certain range of ρ , the proposed algorithm can converge faster with larger ρ values. However, increasing ρ to a too large value will cause numerical instability and divergence.

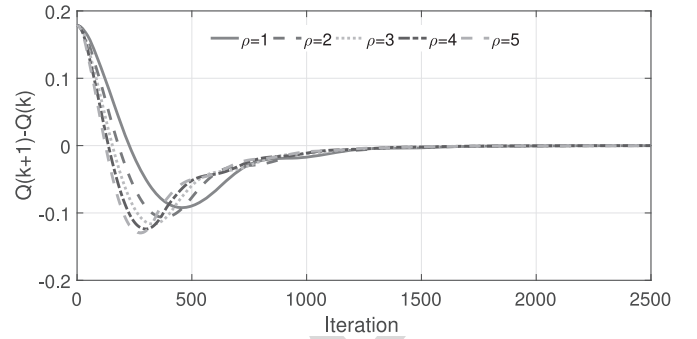


Fig. 4. Convergence of the distributed optimization: Impact of different penalty parameter ρ values.

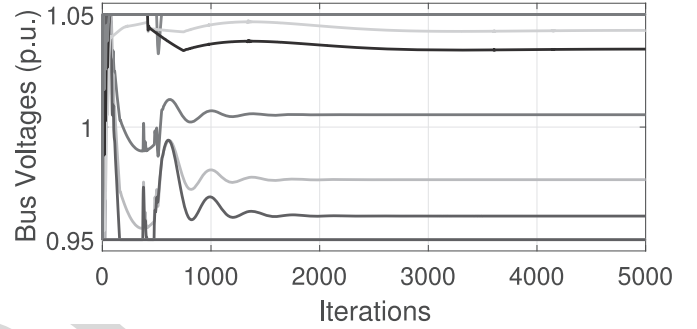


Fig. 5. Convergence of the distributed optimization: Iterative updates of bus voltage magnitudes $\rho=5$.

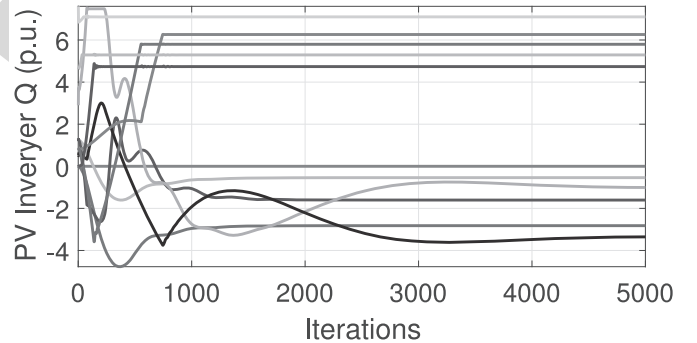


Fig. 6. Convergence of the distributed optimization: Iterative updates of PV inverter reactive power outputs $\rho=5$.

The iterative updates of bus voltages with $\rho = 5$ are shown in Fig. 5. All the optimal voltage magnitudes have converged to values within [0.95 p.u., 1.05 p.u.] interval, which satisfies the bus voltage limit constraints. Fig. 6 presents the iterative updates of three-phase reactive power outputs of PV inverters with $\rho = 5$. It can be seen that most of variables converge after 3000 iterations, while only a few take more than 4000 iterations to converge.

B. Case II: IEEE 34-Bus Distribution System

The results of simulation studies on modified IEEE 34-bus distribution system (Fig. 7) are presented in this section. Details about this test network can be found in [34]. It is assumed that the substation OLTC is within $\pm 10\%$ tap range.

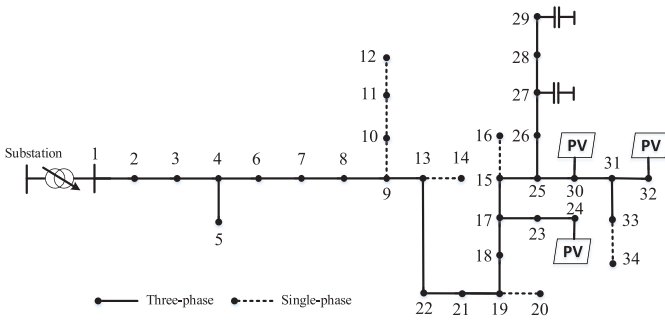


Fig. 7. Case II: Modified IEEE 34-bus test distribution system.

TABLE II
CASE II: BUS TYPE

Type	Residential	Commercial	Industrial
Bus number	2,3,4,5,9,10, 11,12,13,14,16, 17,18,19,20,22, 24,26,28,33,34	15,21, 25,30,31	27,29, 32

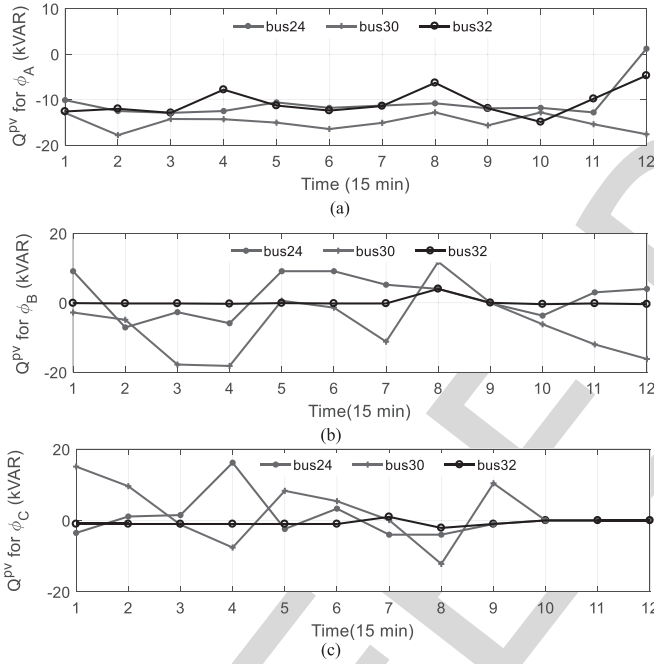


Fig. 8. Case II: Optimal results with full implementation of CVR (a)-(c) PV inverter three-phase reactive power outputs.

TABLE III
CASE II: OPTIMAL RESULTS OF CB SWITCHING STATES AND OLTC TAP POSITIONS

CB position	Hour 1	Hour 2	Hour 3
Bus 27	0	1	0
Bus 29	1	1	1
Substation OLTC	-4	-4	-3

TABLE IV
CASE II: COMPARISON RESULTS BETWEEN CENTRALIZED OPT. AND MODIFIED ADMM

	Centralized Opt.	Modified ADMM
Load reduction	3.79%	3.84%
CPU time	623.0s	235.3s

shows the results of three phase PV inverter reactive power outputs, which change each 15 minutes based on the latest system information. Table III demonstrates that in order to overcome the voltage drop problems caused by CVR effects, the CB on bus 27 is only needed on the second hour of peak load interval, the CB on bus 29 is always on, and the substation OLTC tap position varies between tap -3 and -4 . Note the difference between the decision timescales of PV inverters on the one hand, and CBs/OLTC on the other hand.

A numerical comparison is presented in Table IV between a centralized solver versus the proposed modified distributed ADMM for optimization (10)-(25) tested on the modified 34-bus test system. It can be seen that the percentage of load reduction from the centralized optimization and the proposed modified ADMM are very similar to each other, with ADMM yielding slightly better results. More importantly, the average computational time per agent per iteration of our method is 0.235 seconds and the average convergence iteration is around 1000. Therefore, in terms of computational efficiency, the distributed ADMM takes approximately one third of the computational time of centralized solver to reach comparable and slightly better results. This demonstrates the advantage of the proposed distributed optimization technique for real-time applications. Other computational benefits of ADMM are discussed in detail in [35] and [36].

In the next step, the proposed solution method is applied to the test system model with varying weight factors for the components of the objective function (load reduction versus loss reduction). As discussed before, CVR implementation defines a trade-off between voltage reduction and real power loss reduction, which needs to be numerically quantified. Five different cases, named as *Opt. 1* to *Opt. 5*, are defined with different weight values (w_1, w_2), varying from $(1,0)$, $(0.75,0.25)$, $(0.5,0.5)$, $(0.25,0.75)$ to $(0,1)$. The cases *Opt. 1* to *Opt. 5* represent the variation of objective function from full implementation of bus voltage minimization to full implementation of power loss minimization.

The total energy reduction is calculated as the summation of load power reduction and power loss reduction. The total energy reduction for *Opt. 1* to *Opt. 5* varies from 2.77% to 0.91%. Fig. 9 shows voltage profiles of ϕ_a for all cases, including the base case, in one snapshot. The optimal voltage

Two three-phase CBs are installed at buses 27 and 29, and the CB capacities are the same as the original system. The PV generations are aggregated at buses 24, 30 and 32. It is assumed that the PV at each bus can provide 60% of load at the bus to ensure that the PV capacities and outputs are different from each other. For comparison, a base case without any VVO is defined, where unity-power factor control mode is used for PVs, the tap position of OLTC is fixed, and CB status is on.

The bus types are listed in Table II and the corresponding ZIP load coefficients for different load types are presented in Table I [28]. The proposed modified ADMM method is applied to the test system with full implementation of CVR, which implies the weight factors $w_1 = 1, w_2 = 0$. Fig. 8

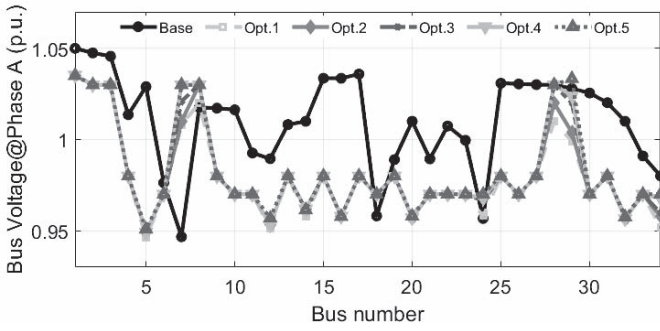
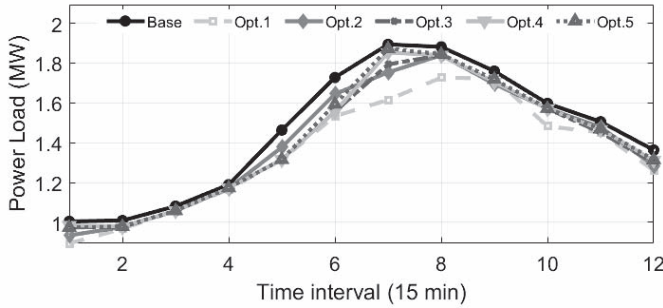
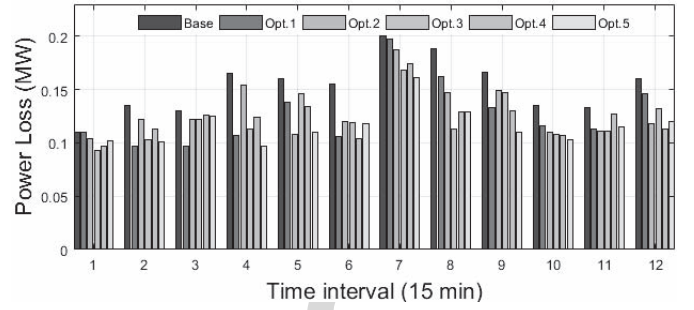

 Fig. 9. Case II: Voltage profiles at $t=1$ and for ϕ_A of base case and cases *Opt. 1* to *Opt. 5*.

 Fig. 10. Case II: Load power consumption for the base case and cases *Opt. 1* to *Opt. 5*.

 Fig. 11. Case II: Power losses for the base case and cases *Opt. 1* to *Opt. 5*.

 TABLE V
 CASE II: SUMMARY OF SYSTEM LOSS, LOAD AND TOTAL ENERGY REDUCTION WITH DIFFERENT ZIP COEFFICIENTS AND WEIGHT FACTORS

Cases	Loss reduction	Load reduction	Total reduction	
ZIP1 (0.4,0.3,0.3)	Opt.1	2.62%	4.07%	3.93%
	Opt.2	4.52%	3.82%	3.89%
	Opt.3	10.21%	3.17%	3.87%
	Opt.4	14.04%	2.62%	3.75%
	Opt.5	18.53%	1.01%	2.74%
ZIP2 (1,0,0)	Opt.1	1.82%	5.53%	5.11%
	Opt.2	4.47%	5.07%	4.95%
	Opt.3	6.47%	4.66%	4.78%
	Opt.4	7.84%	4.12%	4.43%
	Opt.5	9.90%	3.44%	4.01%
ZIP3 (0,0,1)	Opt.1	-3.28%	0.00%	-0.36%
	Opt.2	-1.87%	0.00%	-0.20%
	Opt.3	-1.48%	0.00%	-0.16%
	Opt.4	-0.50%	0.00%	-0.05%
	Opt.5	3.98%	0.00%	0.43%

658 magnitudes of *Opt. 1* to *Opt. 5* are generally lower than the
 659 base case (black solid line), which shows the voltage reduction
 660 effects of VVO. Due to the optimization constraints and
 661 the impacts of reactive power injection from PV inverters and
 662 CBs, the optimal voltage magnitude on a number of buses are
 663 slightly higher than the base case voltages at some non-critical
 664 time points. Comparing the optimal bus voltage magnitudes in
 665 the defined cases, *Opt. 1* shows the lowest bus voltage, which
 666 demonstrates the CVR impact on voltage reduction, as a higher
 667 weight is assigned to voltage minimization component.

668 Fig. 10 and Fig. 11 present the load power consumption and
 669 power losses of the base case and CVR cases *Opt. 1-Opt. 5*,
 670 respectively. As can be observed for the case of *Opt. 1*, the
 671 highest load reduction at peak time is achieved since a higher
 672 weight is assigned to the load reduction objective in equation
 673 (10). Among the cases *Opt. 1-Opt. 5* and the base case,
 674 *Opt. 1* has the largest load reduction and *Opt. 5* has the largest
 675 loss reduction, which shows the effect of various w_1 and w_2 ,
 676 respectively. Hence, it is corroborated that by changing the
 677 weight factors in the optimization model the trade-off between
 678 CVR and loss minimization in the final decision solution can
 679 be controlled effectively.

680 In order to further investigate the impact of CVR on power
 681 losses, three cases with different ZIP coefficients have been
 682 introduced. *ZIP1* represents the general active and reactive ZIP
 683 loads with coefficients [0.4, 0.3, 0.3]. Two extreme cases *ZIP2*
 684 and *ZIP3* represent pure constant impedance active/reactive
 685 loads with coefficients [1, 0, 0], and pure constant power
 686 active/reactive loads with coefficients [0, 0, 1], respectively.
 687 In Table V, loss reduction levels, load reduction levels and

688 total energy reduction have been shown for Case II and under
 689 different ZIP models, *ZIP1*, *ZIP2*, *ZIP3*, and with different
 690 optimization weight assignment scenarios, *Opt. 1-Opt. 5*.

691 Based on the results from Table V and Fig. 12, it can be
 692 observed that for *ZIP1* and *ZIP2*, loss reduction levels are
 693 increasing from *Opt. 5* to *Opt. 1*, however, the load reduction
 694 and total energy reduction decrease at the same time. Since
 695 *ZIP3* represents pure constant power loads, consumption levels
 696 are always the same as the base case regardless of bus voltage
 697 levels, and the loss reduction and total energy reduction
 698 increase for *Opt. 1* to *Opt. 5*. Therefore, for voltage-dependent
 699 loads, *ZIP1* and *ZIP2*, load reduction (due to voltage reduction)
 700 accounts for the majority of the change in total energy
 701 savings. On the other hand, since CVR has no impact on the
 702 constant power loads, *ZIP3*, for that case load reduction is
 703 zero and the loss optimization is the only effective method to
 704 reduce the peak demand.

C. Case III: IEEE 123-Bus Distribution System

705 To test our proposed distributed algorithm on a larger
 706 system, simulation results for modified IEEE 123-bus distribution
 707 system (Fig. 13) with a higher number of PV inverters,
 708 CBs and OLTCs are shown in this section. Details about this
 709 test network can be found in [34]. The locations of OLTCs
 710

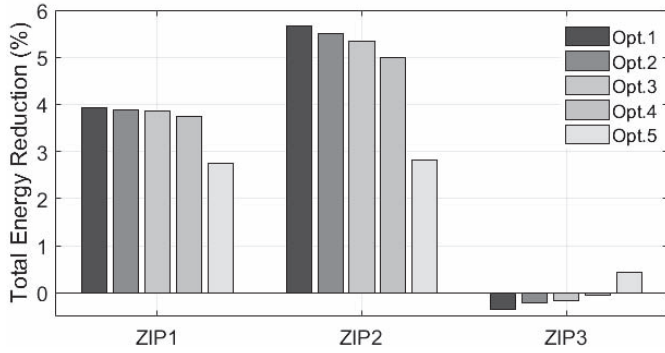


Fig. 12. Case II: Total energy reduction with different ZIP coefficients of base case and cases Opt.1 to Opt.5.

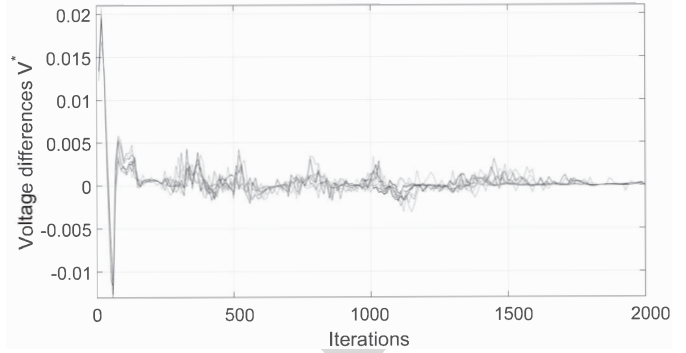


Fig. 14. Convergence of the distributed optimization: bus voltage residues at each iteration.

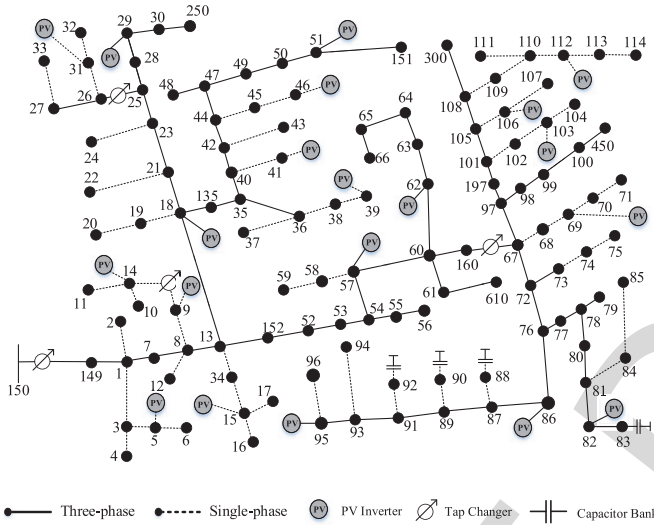


Fig. 13. Case III: Modified IEEE 123-bus test distribution system.

TABLE VI
CASE III: LOCATIONS AND CAPACITIES OF DEVICES

Type	Locations	Capacities
PV	5, 9, 14, 15, 18, 29, 31, 39, 41, 46, 51, 57, 62, 69, 82, 86, 95, 103, 106, 112	20 kVAr per ϕ_a, ϕ_b, ϕ_c
CB	83, 88, 90, 92	{200, 200, 200}, {50, 0, 0}, {50, 0, 0}, {50, 0, 0} kVAr
OLTC	9, 25, 120, 150	Tap $\in \{-10, -9 \dots 0 \dots 9, 10\}$

are set to be the same as [18]. The locations and capacities of CB are selected based on the original settings in [34]. The locations of PV are adopted from [37]. Table VI summarizes the types, locations and capacities of the devices integrated in the system.

The proposed method is applied to the modified 123-bus test system with ZIP coefficients [0.4, 0.3, 0.3] for both active and reactive loads, and full implementation of CVR ($w_1 = 1$). In order to show the convergence process, Fig. 14 shows the average iteration-wise updates in voltage magnitude, i.e., $V_{i,t,\phi}^*(k) = V_{i,t,\phi}(k+1) - V_{i,t,\phi}(k)$ with k being the iteration index. It can be seen that voltage residues V^* converge to zero as the iteration number, k , increases. Hence, the algorithm

TABLE VII
CASE III: SUMMARY OF LOSS, LOAD AND TOTAL ENERGY REDUCTION WITH DIFFERENT ZIP FACTORS AND WEIGHT FACTORS

Cases	Loss reduction	Load reduction	Total reduction	
ZIP1 (0.4,0.3,0.3)	Opt.1	4.60%	6.32%	6.20%
	Opt.2	6.29%	5.36%	5.42%
	Opt.3	8.53%	4.08%	4.39%
	Opt.4	11.72%	2.98%	3.58%
	Opt.5	14.05%	2.23%	3.04%
ZIP2 (1,0,0)	Opt.1	3.68%	9.68%	9.27%
	Opt.2	5.81%	9.13%	8.91%
	Opt.3	8.19%	8.48%	8.46%
	Opt.4	10.34%	7.41%	7.61%
	Opt.5	12.79%	6.65%	7.07%
ZIP3 (0,0,1)	Opt.1	-6.34%	0.00%	-1.20%
	Opt.2	-5.89%	0.00%	-1.12%
	Opt.3	-5.65%	0.00%	-1.07%
	Opt.4	-1.52%	0.00%	-0.29%
	Opt.5	2.70%	0.00%	0.51%

converges to optimal solution within an acceptable number of iterations in a reasonable time. Based on our numerical experiments, the average computational time per agent per iteration for the IEEE 123-bus system is 0.245 seconds. Hence, the overall algorithm takes around 6 minutes to converge (ignoring communication delays) for this test system. On the other hand, the selected time step for the simulation is $t = 15$ minutes, which is well above the required algorithm convergence time. Hence, the distributed algorithm is well capable of reaching the solution within the selected decision time step. Another reason that a time step of 15 minutes was selected is that this time step is consistent with the frequency measurement of current smart meters used in the industry.

In Table VII, the total network loss reduction, load reduction and total energy for different categories of load, ZIP1, ZIP2, and ZIP3, have been shown as a function of different weight values assigned to optimization objective components. As can be seen in this table, similar trends are observed as those of the smaller case study (Case II) shown in Table V: for voltage-dependent loads ZIP1 and ZIP2, loss reduction levels increase from Opt. 1 through Opt. 5, and the load reduction and total energy reduction decrease in Opt. 1 through Opt. 5; for constant power load ZIP3, load consumption levels are always

747 the same as the base case, and the loss reduction and total
 748 energy reduction increase in *Opt. 1* through *Opt. 5*. In addi-
 749 tion, more load reduction is achieved for this case. Therefore,
 750 the conclusions drawn in Section IV-B regarding the trade-
 751 off between voltage magnitude optimization and network loss
 752 reduction under different ZIP characteristics are again verified
 753 for the larger IEEE 123-bus test system.

754 V. CONCLUSION

755 A distributed method is developed to optimally coordinate
 756 the fast-dispatch of PV inverters with the slow-dispatch of
 757 OLTC and CBs for CVR in three-phase unbalanced distribu-
 758 tion systems. The trade-off between voltage reduction (load
 759 reduction) and real power loss minimization is analyzed by
 760 the developed multi-objective VVO formulation. The proposed
 761 VVO-based CVR is solved by distributed optimization algo-
 762 rithm ADMM, which can maintain customer data privacy
 763 and alleviate computational burden in large-scale distribution
 764 networks. In order to better handle the non-convexity of the
 765 decision problem caused by discrete variables, the distributed
 766 algorithm ADMM is modified in a way that the discrete vari-
 767 ables are not only relaxed into continuous variables, but also
 768 implemented as a generalized part of the objective function
 769 in the iterations to avoid sub-optimality. According to case
 770 studies, our proposed method can converge within an accept-
 771 able number of iterations for large unbalanced distribution
 772 systems. It is also observed that different load types affect the
 773 CVR performance differently. Among different load types, the
 774 highest levels of the CVR-based consumption reduction are
 775 achieved for voltage-sensitive loads. Also it is demonstrated
 776 that as the penetration of voltage-sensitive customers increases,
 777 CVR could be a better option for energy saving at substation
 778 level during peak load interval, compared to mere network loss
 779 minimization.

780 REFERENCES

781 [1] D. Kirshner, "Implementation of conservation voltage reduction at
 782 commonwealth edison," *IEEE Trans. Power Syst.*, vol. 5, no. 4,
 783 pp. 1178–1182, Nov. 1990.
 784 [2] Z. Wang and J. Wang, "Time-varying stochastic assessment of conser-
 785 vation voltage reduction based on load modeling," *IEEE Trans. Power*
 786 *Syst.*, vol. 29, no. 5, pp. 2321–2328, Sep. 2014.
 787 [3] G. W. Kim and K. Y. Lee, "Coordination control of ULTC transformer
 788 and STATCOM based on an artificial neural network," *IEEE Trans.*
 789 *Power Syst.*, vol. 20, no. 2, pp. 580–586, May 2005.
 790 [4] J.-Y. Park, S.-R. Nam, and J.-K. Park, "Control of a ULTC considering
 791 the dispatch schedule of capacitors in a distribution system," *IEEE Trans.*
 792 *Power Syst.*, vol. 22, no. 2, pp. 755–761, May 2007.
 793 [5] T. V. Dao, S. Chaitusaney, and H. T. N. Nguyen, "Linear least-squares
 794 method for conservation voltage reduction in distribution systems
 795 with photovoltaic inverters," *IEEE Trans. Smart Grid*, vol. 8, no. 3,
 796 pp. 1252–1263, May 2017.
 797 [6] C. Zhang, Y. Xu, Z. Y. Dong, and J. Ravishankar, "Three-stage robust
 798 inverter-based voltage/var control for distribution networks with high-
 799 level PV," *IEEE Trans. Smart Grid*, to be published.
 800 [7] Y. Xu, Z. Y. Dong, R. Zhang, and D. J. Hill, "Multi-timescale coordi-
 801 nated voltage/var control of high renewable-penetrated distribution
 802 systems," *IEEE Trans. Power Syst.*, vol. 32, no. 6, pp. 4398–4408,
 803 Nov. 2017.
 804 [8] B. Zhang, A. Y. S. Lam, A. D. Domínguez-García, and D. Tse, "An
 805 optimal and distributed method for voltage regulation in power distribu-
 806 tion systems," *IEEE Trans. Power Syst.*, vol. 30, no. 4, pp. 1714–1726,
 807 Jul. 2015.

[9] N. Mahmud and A. Zahedi, "Review of control strategies for voltage
 808 regulation of the smart distribution network with high penetration of
 809 renewable distributed generation," *Renew. Sustain. Energy Rev.*, vol. 64,
 810 pp. 582–595, Oct. 2016.
 811 [10] C. R. Sarimuthu, V. K. Ramachandaramurthy, K. R. Agileswari, and
 812 H. Mokhlis, "A review on voltage control methods using on-load tap
 813 changer transformers for networks with renewable energy sources,"
 814 *Renew. Sustain. Energy Rev.*, vol. 62, pp. 1154–1161, Sep. 2016.
 815 [11] D. K. Molzahn *et al.*, "A survey of distributed optimization and control
 816 algorithms for electric power systems," *IEEE Trans. Smart Grid*, vol. 8,
 817 no. 6, pp. 2941–2962, Nov. 2017.
 818 [12] H. J. Liu, W. Shi, and H. Zhu, "Hybrid voltage control in distribution
 819 networks under limited communication rates," *IEEE Trans. Smart Grid*,
 820 to be published.
 821 [13] Q. Zhang and M. Sahraei-Ardakani, "Impacts of communication limits
 822 on convergence of distributed DCOPF with flexible transmission," in
 823 *Proc. North Amer. Power Symp. (NAPS)*, Sep. 2017, pp. 1–6.
 824 [14] Y. Wang, S. Wang, and L. Wu, "Distributed optimization approaches for
 825 emerging power systems operation: A review," *Elect. Power Syst. Res.*,
 826 vol. 144, pp. 127–135, Mar. 2017.
 827 [15] Q. Zhang and M. Sahraei-Ardakani, "Distributed DCOPF with flexible
 828 transmission," *Elect. Power Syst. Res.*, vol. 154, pp. 37–47, Jan. 2018.
 829 [16] Q. Peng and S. H. Low, "Distributed algorithm for optimal power flow
 830 on a radial network," in *Proc. IEEE 53rd Annu. Conf. Decis. Control*
 831 *(CDC)*, Los Angeles, CA, USA, 2014, pp. 167–172.
 832 [17] Q. Peng and S. H. Low, "Distributed optimal power flow algorithm for
 833 radial networks, I: Balanced single phase case," *IEEE Trans. Smart Grid*,
 834 vol. 9, no. 1, pp. 111–121, Jan. 2018.
 835 [18] B. A. Robbins, H. Zhu, and A. D. Domínguez-García, "Optimal
 836 tap setting of voltage regulation transformers in unbalanced distribu-
 837 tion systems," *IEEE Trans. Power Syst.*, vol. 31, no. 1, pp. 256–267,
 838 Jan. 2016.
 839 [19] B. A. Robbins and A. D. Domínguez-García, "Optimal reactive power
 840 dispatch for voltage regulation in unbalanced distribution systems," *IEEE*
 841 *Trans. Power Syst.*, vol. 31, no. 4, pp. 2903–2913, Jul. 2016.
 842 [20] P. Šulc, S. Backhaus, and M. Chertkov, "Optimal distributed control of
 843 reactive power via the alternating direction method of multipliers," *IEEE*
 844 *Trans. Energy Convers.*, vol. 29, no. 4, pp. 968–977, Dec. 2014.
 845 [21] J. Eckstein, "Parallel alternating direction multiplier decomposition of
 846 convex programs," *J. Optim. Theory Appl.*, vol. 29, no. 4, pp. 968–977,
 847 2014.
 848 [22] Q. Liu, X. Shen, and Y. Gu, "Linearized ADMM for non-convex
 849 non-smooth optimization with convergence analysis," *arXiv preprint*
 850 *arXiv:1705.02502*, 2017.
 851 [23] C. He, L. Wu, T. Liu, and M. Shahidehpour, "Robust co-optimization
 852 scheduling of electricity and natural gas systems via ADMM," *IEEE*
 853 *Trans. Sustain. Energy*, vol. 8, no. 2, pp. 658–670, Apr. 2017.
 854 [24] A. Alavian and M. C. Rotkowitz, "Improving ADMM-based
 855 optimization of mixed integer objectives," in *Proc. 51st Annu. Conf.*
 856 *Inf. Sci. Syst. (CISS)*, Baltimore, MD, USA, Mar. 2017, pp. 1–6.
 857 [25] *Evaluation of Conservation Voltage Reduction on a National Level*,
 858 Pac. Northwest Nat. Lab., Richland, WA, USA. [Online]. Available:
 859 [https://www.pnnl.gov/main/publications/external/technical_reports/](https://www.pnnl.gov/main/publications/external/technical_reports/PNNL-19596.pdf)
 860 [PNNL-19596.pdf](https://www.pnnl.gov/main/publications/external/technical_reports/PNNL-19596.pdf)
 861 [26] Z. Wang, M. Begovic, and J. Wang, "Analysis of conservation voltage
 862 reduction effects based on multistage SVR and stochastic process," *IEEE*
 863 *Trans. Smart Grid*, vol. 5, no. 1, pp. 431–439, Jan. 2014.
 864 [27] Z. Wang, J. Wang, B. Chen, M. M. Begovic, and Y. He, "MPC-based
 865 voltage/var optimization for distribution circuits with distributed gener-
 866 ators and exponential load models," *IEEE Trans. Smart Grid*, vol. 5,
 867 no. 5, pp. 2412–2420, Sep. 2014.
 868 [28] M. Diaz-Aguiló *et al.*, "Field-validated load model for the analysis of
 869 CVR in distribution secondary networks: Energy conservation," *IEEE*
 870 *Trans. Power Del.*, vol. 28, no. 4, pp. 2428–2436, Oct. 2013.
 871 [29] A. Bokhari *et al.*, "Experimental determination of the ZIP coefficients
 872 for modern residential, commercial, and industrial loads," *IEEE Trans.*
 873 *Power Del.*, vol. 29, no. 3, pp. 1372–1381, Jun. 2014.
 874 [30] C. Yang, A. A. Thatte, and L. Xie, "Multitime-scale data-driven spatio-
 875 tiotemporal forecast of photovoltaic generation," *IEEE Trans. Sustain.*
 876 *Energy*, vol. 6, no. 1, pp. 104–112, Jan. 2015.
 877 [31] Z. Wang and J. Wang, "Review on implementation and assessment of
 878 conservation voltage reduction," *IEEE Trans. Power Syst.*, vol. 29, no. 3,
 879 pp. 1306–1315, May 2014.
 880 [32] D. Lauria, "Conservation voltage reduction (CVR) at northeast utili-
 881 ties," *IEEE Trans. Power Del.*, vol. PWRD-2, no. 4, pp. 1186–1191,
 882 Oct. 1987.
 883

- 884 [33] A. Dwyer, R. E. Nielsen, J. Stangl, and N. S. Markushevich, "Load
885 to voltage dependency tests at B.C. hydro," *IEEE Trans. Power Syst.*,
886 vol. 10, no. 2, pp. 709–715, May 1995.
- 887 [34] W. H. Kersting, "Radial distribution test feeders," in *Proc. IEEE Power
888 Eng. Soc. Win. Meeting*, vol. 2, 2001, pp. 908–912.
- 889 [35] E. Dall'Anese, H. Zhu, and G. B. Giannakis, "Distributed optimal power
890 flow for smart microgrids," *IEEE Trans. Smart Grid*, vol. 4, no. 3,
891 pp. 1464–1475, Sep. 2013.
- 892 [36] S. P. Boyd, N. Parikh, E. Chu, B. Peleato, and J. Eckstein, "Distributed
893 optimization and statistical learning via the alternating direction method
894 of multipliers," *Found. Trends® Mach. Learn.*, vol. 3, no. 1, pp. 1–122,
895 2011.
- 896 [37] Z. Wang and J. Wang, "Self-healing resilient distribution systems based
897 on sectionalization into microgrids," *IEEE Trans. Power Syst.*, vol. 30,
898 no. 6, pp. 3139–3149, Nov. 2015.



Kaveh Dehghanpour (S'14–M'17) received the B.Sc. and M.S. degrees in electrical and computer engineering from the University of Tehran in 2011 and 2013, respectively, and the Ph.D. degree in electrical engineering from Montana State University in 2017. He is currently a Post-Doctoral Research Associate with Iowa State University. His research interests include application of machine learning and data-driven techniques in power system monitoring and control.



Zhaoyu Wang (S'13–M'15) received the B.S. and first M.S. degrees in electrical engineering from Shanghai Jiaotong University in 2009 and 2012, respectively, and the second M.S. and Ph.D. degrees in electrical and computer engineering from the Georgia Institute of Technology in 2012 and 2015, respectively. He is a Harpole-Pentair Assistant Professor with Iowa State University. He was a Research Aid with Argonne National Laboratory in 2013 and an Electrical Engineer Intern with Corning Inc. in 2014. His research interests include

power distribution systems, microgrids, renewable integration, power system resilience, and power system modeling. He is the Principal Investigator for a multitude of projects focused on these topics and funded by the National Science Foundation, the Department of Energy, National Laboratories, PSERC, and Iowa Energy Center. He was a recipient of the IEEE Power and Energy Society (PES) General Meeting Best Paper Award in 2017 and the IEEE Industrial Application Society Prize Paper Award in 2016. He is the Secretary of IEEE PES Award Subcommittee. He is an Editor of the IEEE TRANSACTIONS ON SMART GRID and IEEE PES LETTERS.



Qianzhi Zhang (S'17) received the B.S. degree in electrical and computer engineering from the Shandong University of Technology in 2012 and the M.S. degree in electrical and computer engineering from Arizona State University in 2015. He is currently pursuing the Ph.D. degree with the Department of Electrical and Computer Engineering, Iowa State University, Ames, IA, USA. From 2015 to 2016, he was a Research Engineer with Huadian Electric Power Research Institute, Hangzhou, China. His research interests include power distribution

systems, microgrids, applications of distributed optimization, and machine learning in power systems.

IEEE P